Quantum oscillations in the magnetic Weyl semimetal NdAlSi arising from strong Weyl fermion–4f electron exchange interaction

Jin-Feng Wang,[1,2] Qing-Xin Dong,[1,3] Yi-Fei Huang,[1,3] Zhao-Sheng Wang,[4] Zhao-Peng Guo,[1,3] Zhi-Jun Wang,[1,3,5] Zhi-An Ren,[1,3,5] Gang Li,[1,3,5,*] Pei-Jie Sun,[1,3,5,†] Xi Dai,[1,6,7,‡] and Gen-Fu Chen[1,3,5,§]

[1]*Institute of Physics and Beijing National Laboratory for Condensed Matter Physics, Chinese Academy of Sciences, Beijing 100190, China*
[2]*Henan Normal University, School of Physics, Henan Province Key Laboratory of Photovoltaic Materials, Xinxiang, Henan 453007, China*
[3]*School of Physical Sciences, University of Chinese Academy of Sciences, Beijing 100049, China*
[4]*Anhui Province Key Laboratory of Condensed Matter Physics at Extreme Conditions, High Magnetic Field Laboratory of the Chinese Academy of Sciences, Hefei, Anhui 230031, China*
[5]*Songshan Lake Materials Laboratory, Dongguan, Guangdong 523808, China*
[6]*Materials Department, University of California, Santa Barbara, California 93106-5050, USA*
[7]*Department of Physics, The Hongkong University of Science and Technology, Clear Water Bay, Kowloon 999077, Hong Kong, China*

(Received 11 April 2022; revised 9 January 2023; accepted 28 June 2023; published 24 July 2023)

Magnetic topological materials are a realization of topologically nontrivial electronic band structure with magnetic correlation effects; they offer novel opportunities in manipulating charge/spin transport as well as spin texture. In the search for emergent phenomena that are specific in this class of materials, here we report on a type of quantum oscillation of a polar magnetic Weyl semimetal (WSM) NdAlSi in both the temperature dependent electrical resistivity and specific heat at a constant magnetic field. It is revealed that they arise from the destructive interference between field dependent quantum oscillations of the spin-split Fermi surfaces due to the strong Weyl fermion–4f electron exchange interaction combined with Rashba-Dresselhaus and Zeeman effects. Our results demonstrate that the f electrons bearing magnetic WSMs possess even richer responses to external stimuli compared to known d-electron magnetic WSMs and call for further in-depth investigations.

DOI: 10.1103/PhysRevB.108.024423

I. INTRODUCTION

The ternary R-Al-B (R: Ce, Pr, Nd, Sm; B: Ge or Si) compounds are recently recognized as Weyl semimetals that break both inversion and time-reversal symmetries. They offer a rare, unambiguous platform to explore exotic quantum phenomena arising from the interplay between magnetism, electronic correlations, and topology [1–8]. Recent studies of NdAlSi revealed that its helical magnetic order is driven by Weyl-mediated exchange interactions, providing an example of Weyl fermions promoting collective magnetism [9,10]. The compound hosts a complex temperature–magnetic field phase diagram and peculiar magnetotransport behaviors [10,11]. Intriguingly, Weyl fermions survive in NdAlSi not only below but also above T_N under applied magnetic fields, suggesting a possible unconventional paramagnetic state that emerges from the suppression of magnetic order. Moreover, the energy splitting between the f-electron ground state doublet and four excited doublets due to crystal electric field (CEF) is rather small, ∼4.1 meV, indicating that the excited multiplets can mix easily into the ground state by applying magnetic field [10].

In this work, we report the experimental observation of a different presentation of quantum oscillations in NdAlSi. We find that both the electrical resistivity and specific heat oscillate as a function of temperature at a constant magnetic field, in addition to the conventional magnetic field dependent quantum oscillations at a constant temperature. Furthermore, we propose a phenomenological model to quantitatively account for the unique quantum oscillations observed herein, by including the spin-split Fermi surfaces due to the strong Weyl fermion –f electron exchange interaction.

II. RESULTS AND DISCUSSION

NdAlSi crystallizes in the noncentrosymmetric space group $I4_1md$, with a body centered tetragonal unit cell [11]. Figure 1(a) illustrates the temperature dependent resistivity at various magnetic fields ($T < 100$ K; $B > B_C$, B_C: The metamagnetic transition field) [11]. All of them exhibit oscillatory features, which shift towards the high temperature region with enhanced amplitude by increasing magnetic field. The anomalous component, obtained by subtracting a smooth background, is plotted versus logarithmic temperature in Fig. 1(b). The most striking feature is that the spindlelike oscillations are periodiclike in $\log T$. These spindles mirror the rise and decline of oscillation aptitudes and reflect the dramatic changes in the potential across a critical regime. As shown in Fig. 1(c), the saturation behaviors of $M(B > B_c)$ at low temperatures evince the complete polarization of Nd^{3+}

*gli@iphy.ac.cn
†pjsun@iphy.ac.cn
‡daix@ucsb.edu
§gfchen@iphy.ac.cn

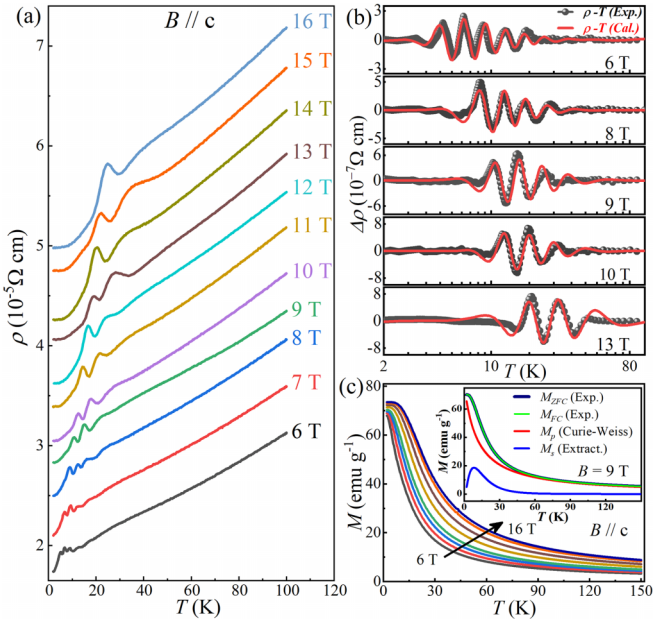

FIG. 1. Temperature dependent magnetoresistivity oscillations and high-field magnetization of NdAlSi. (a) Resistivity vs temperature ($\rho-T$) curves under constant magnetic fields. The curves are vertically shifted for clarity. (b) Extracted $\Delta\rho-T$ oscillations (black dotted lines) and their fitting results (red lines) for $B = 6$, 8, 9, 10, and 13 T. (c) Temperature dependent zero-field-cooled (ZFC) magnetization. Inset: The comparison of $M_{\rm ZFC}$ (deep blue) and $M_{\rm FC}$ (green) measured at $B = 9$ T, together with the spin component M_s (blue) by subtracting the Curie-Weiss term M_p (red). Note: NdAlSi here is not the same one reported in our previous work cited as Ref. [11].

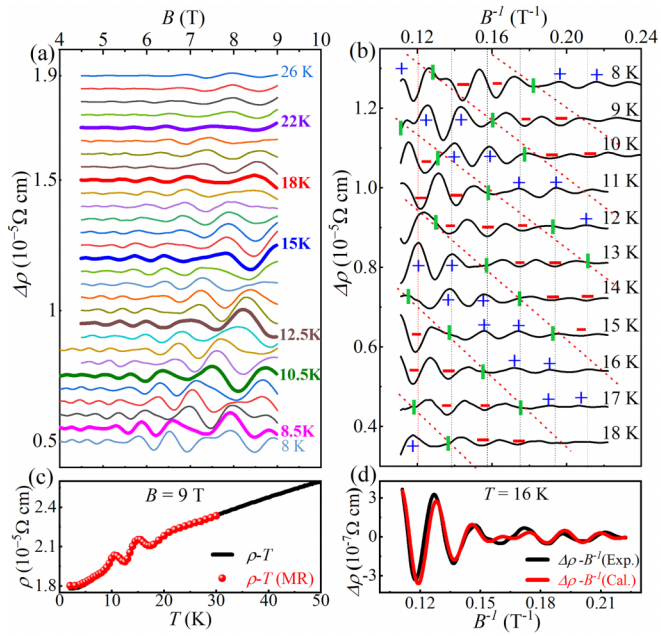

FIG. 2. Exploration of the $\Delta\rho-T$ oscillations' origin based on SdH oscillations. (a) Stacked isothermal SdH oscillations. (b) $1/B$ dependent SdH oscillations (8–18 K). The phase inversion positions were labeled by green vertical bars. (c) The directly observed $\rho(T)$ curve matches well with the extracted one from the MR data. (d) The observed SdH oscillation at 16 K and its simulation by $\Delta\rho = 2A(B,T)\cos[2\pi(\frac{F}{B}+\phi')]\cos[\pi(\frac{\alpha M(B,T)+\Delta_0}{B}+\mathcal{G})]$, which gives $F = 55$ T and $\Delta_0 = 24$ T.

moments, which destroys the antiferromagnetism in NdAlSi at $B_c \sim 5.2$ T for $B//c$, and results in a field-polarized paramagnetic (PPM) state [12,13]. By subtracting the Curie-Weiss term (M_p) from the measured one [Fig. 1(c) inset], the remaining component M_s shows a nonmonotonic temperature dependence with its peak concurring with the oscillating resistivity. This gives an indication that the interesting oscillatory feature correlates with the spin polarization of f electrons in NdAlSi.

To get more insight into the origin of such a phenomenon, Fig. 2(a) shows the Shubnikov–de Haas (SdH) oscillations for NdAlSi at different temperatures ($T > T_N$), obtained by subtracting a smooth background from isothermal magnetoresistance (MR) data. Gradual variations of the oscillation spectra combined with phase inversions are clearly observed. Especially, the bold-marked curves with different temperatures show 180° out of phase with each other over the measured magnetic field range; such a strong shift of the SdH oscillations' maxima/minima with temperature is not commonly observed in the absence of a temperature driven phase transition. To clarify the beatinglike patterns of the oscillations, we plot $\Delta\rho$ vs $1/B$ in Fig. 2(b). As the results show, the phase inversions occur exactly at the positions of the nodes, i.e., the phase of the SdH oscillations remains the same between adjacent nodes and changes by π after passing the nodal point. The beating effect observed in the quantum oscillations is usually due to the existence of two comparable frequencies with similar amplitudes due to level splitting, and the nodal positions are controlled by the difference of the two

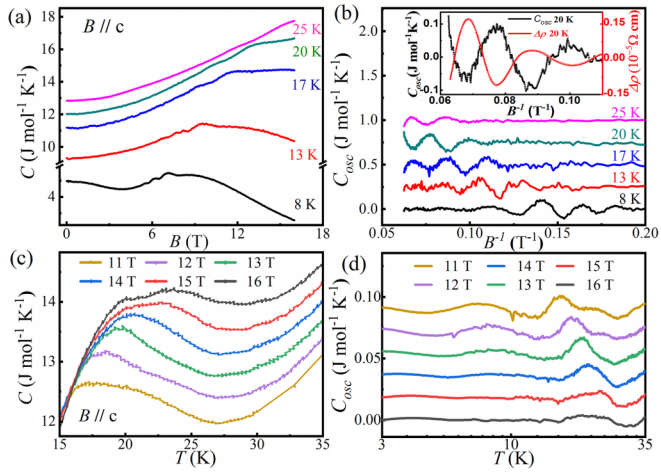

FIG. 3. Specific heat oscillations in NdAlSi. (a) C-B curves at selected temperatures. (b) Extracted $C_{\rm osc}$-$1/B$ oscillations. Inset: A 180° phase inversion occurs between $C_{\rm osc}$-$1/B$ and $\Delta\rho-1/B$ oscillations. (c) C-T curves under several magnetic fields. A broad hump (CEF anomaly) of C shifts to high temperature with increasing magnetic field. (d) $C_{\rm osc}$-T oscillations for selected magnetic fields. The $C_{\rm osc}$ curves in (b) and (d) are vertically shifted by 0.25 and 0.02 J mol^{-1} K^{-1} respectively for clarity.

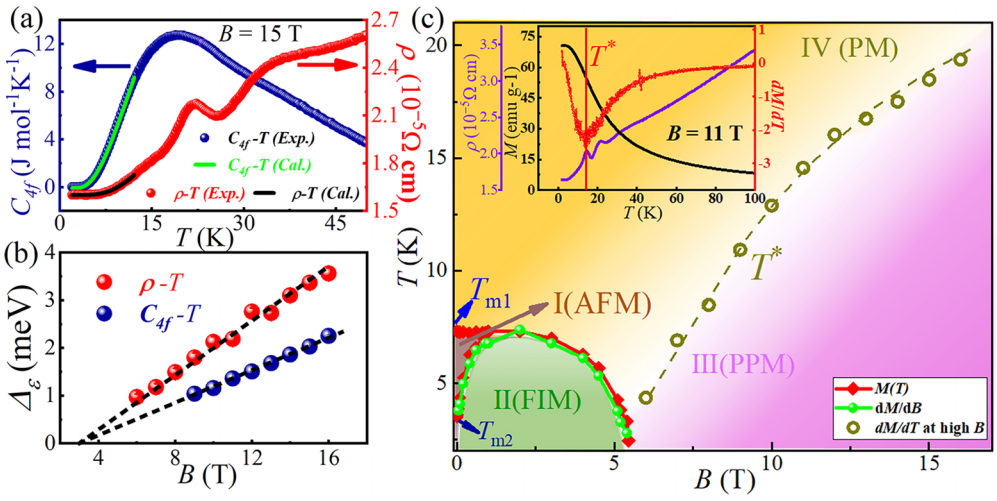

FIG. 4. Low-temperature magnetic excitations and magnetic phase diagram for $B//c$. (a) Typical C_{4f}-T and $\rho-T$ curves for $B = 15$ T ($C_{4f} = C_{NAS} - C_{LAS}$). The green and red lines are the fitting results by $C_{4f} = Ae^{-\Delta\varepsilon/T}$ and $\rho = Ae^{-\Delta\varepsilon/T} + \rho_0$, respectively. (b) Magnetic-field dependencies of the calculated magnetic-excitation gap Δ_ε, which tend to merge at $B_c^* \sim 3$ T. (c) An extended T-B phase diagram of NdAlSi based on our previous report [11], characterized by a crossover at T^* between the PM and PPM phases. Inset: Low-temperature ρ, M, and dM/dT for $B = 11$ T, where T^* is defined as the inflection point in dM/dT. The oscillations appear only in a limited temperature range where the magnetization changes drastically.

spin (up and down) subdensities [14–17]. However, spin splitting zeros in our case are not perfect. Most strikingly, there is a large shift of the nodal position with temperature [Fig. 2(b)]. As shown in the Appendix, Figs. 9 and 13, although the frequencies observed in NdAlSi and LaAlSi are similar, there is no obvious shift of the peak and valley positions of quantum oscillations for LaAlSi [18]. This fact suggests that the $4f$ electrons of Nd in NdAlSi substantially affect the quantum oscillations through exchange coupling with the conduction electrons, i.e., Weyl fermions. Moreover, we also analyze comparatively the data taken from the isothermal MR (Fig. 8) with the directly measured $\rho(T)$ curve. As shown in Fig. 2(c), the two curves are identical, demonstrating that the unexpected temperature-driven resistivity oscillations arise from the destructive interference between two quantum oscillations originating from the Fermi surface splitting, accompanied by a strongly temperature- and magnetic field dependent phase inversion.

Consider here the oscillatory magnetoresistance using the Lifshitz-Kosevich (LK) formula [19,20],

$$\Delta\rho = \left(\frac{B}{2F}\right)^{1/2} R_T R_D R_S \cos\left[2\pi\left(\frac{F}{B} + \gamma - \delta\right)\right], \quad (1)$$

where F is the oscillation frequency, and $\gamma = \frac{1}{2} - (\varphi_B/2\pi)$ is the Onsager phase factor taking the value $\gamma = 0$, 1 (or $\gamma = 1/2$) for the nontrivial (trivial) Berry phase φ_B. The phase shift δ is determined by the dimensionality, i.e., $\delta = \pm 1/8$ for the 3D systems; $R_T = \alpha T m^*/B \sinh(\alpha T m^*/B)$ and $R_D = \exp(-\alpha T_D m^*/B)$ are thermal and Dingle damping factors caused by the finite-temperature effect on the Fermi-Dirac distribution and the electron scattering, respectively. $R_s = \cos(\pi \frac{\Delta E}{\hbar\omega_c})$ is the spin damping factor due to Zeeman splitting, where $\hbar\omega_c$ is the Landau level separation energy and ΔE is the energy splitting of each Landau level. In the conventional linear Zeeman effect, $\Delta E = g\mu_B B$ (g: g factor), and thus $R_S = \cos(\pi g m^*/2m_e)$ becomes independent of B. The so called "spin zeros" will appear as $gm^*/m_e = 2n + 1$ (n is an integer and m^* is the effective mass of electrons), and the g factor could then be obtained. Note that the above spin factor $R_S = \cos(\pi g m^*/2m_e)$ is obtained for free nonrelativistic electrons with parabolic band dispersion, while for a Dirac cone, the energies of Landau levels, $E_n = \sqrt{2\hbar e v_F^2 nB}$, are not equally spaced (v_F: The Fermi velocity of the system with linear dispersion) and the energy separations are dependent on $\sqrt{B}$ [21,22]. Hence $R_s = \cos(\pi \frac{\Delta E}{\hbar\omega_c})$ will be field dependent, leading to a beating pattern in oscillations at half-integer values of $\Delta E/\hbar\omega_c$.

In NdAlSi, in addition to the Zeeman splitting, the asymmetric Rashba-Dresselhaus (RD) interaction, driven by spin-orbit coupling (SOC) in the absence of inversion symmetry, also induces a density imbalance between spin-up and spin-down electronic subbands even at $B = 0$. However, both Zeeman and RD effects cannot explain the observed shifting of nodal positions with temperature [18,23]. Therefore, an additional exchange splitting [24–26] stemming from exchange interaction between the conduction electrons (i.e., Weyl fermions) and the localized $4f$ electrons of Nd [9,10] appears to be crucial in causing the change of band splitting with temperature. Usually, the exchange interaction acts as an effective field that results in populations of spin-up and spin-down quasiparticles that are no longer equal, preventing a regular interference between oscillations from the two spin bands. This leads to the absence of a perfect spin splitting zero in the oscillation patterns and is consistent with the observation in NdAlSi. Therefore, the total spin splitting energy ΔE in NdAlSi under external magnetic field should be a combination of RD spin splitting, Zeeman splitting, and c-f exchange splitting energies.

In such a case, the spin split zeros will appear as $g_{\text{eff}} m^*/m_e = 2n + 1$, if we introduce an effective g factor,

$g_{\text{eff}} = \frac{1}{\mu_0\mu_B}(\frac{dE_{F\uparrow}}{dH} - \frac{dE_{F\downarrow}}{dH})$. Unfortunately, due to the complicated structure of spin nodes and the limited number of spin nodes available, it is not yet possible to describe the variation of the spin damping factor in NdAlSi, although the R_S term provides also a handle for estimating the exchange interaction. An effective assessment of R_S, as well as the resultant g factor (large and tunable), might be a big challenge, and remains a subject of further theoretical and experimental studies.

Alternatively, we herein develop a simple phenomenological model to capture the temperature dependent oscillations without going into the microscopic details of the damping factor in NdAlSi, by considering that the exchange interaction is determined by the magnetization. In general cases, the LK formula (1) could be reformulated as

$$\Delta\rho = A(B,T)\cos\left[2\pi\left(\frac{F}{B}+\varphi\right)\right], \tag{2}$$

where $A(B, T)$ is the SdH oscillation amplitude governed by both thermal broadening and impurity scattering. Due to the Fermi surface splitting, the SdH frequency F is split into two comparable frequencies, F_+ and F_-, and thus the conventional LK Eq. (2) could be modified as the following:

$$\begin{aligned}\Delta\rho =& A_1(B,T)\cos\left[2\pi\left(\frac{F_+}{B}\right)+\phi_+ +\pi\mathcal{G}_+ +\xi\right]\\ &+A_2(B,T)\cos\left[2\pi\left(\frac{F_-}{B}\right)+\phi_- +\pi\mathcal{G}_- +\xi\right],\end{aligned} \tag{3}$$

where $\mathcal{G}_+$ and $\mathcal{G}_-$ represent the spin states arising from the Zeeman splitting and $\boldsymbol{\xi}$ is the field independent phase stemming from the RD splitting. For simplicity, considering $\mathcal{G}_+ + \mathcal{G}_- = 0, \mathcal{G} = \mathcal{G}_+ - \mathcal{G}_- = gm^*/2m_e$, and the amplitude and frequency that are spin independent, summing over the Eq. (3) yields

$$\Delta\rho = 2A(B,T)\cos\left[2\pi\left(\frac{F}{B}+\phi'\right)\right]\cos\left[\pi\left(\frac{\Delta F}{B}+\mathcal{G}\right)\right], \tag{4}$$

where $F = (F_+ + F_-)/2$, $\Delta F = F_+ - F_-$. Since the frequency difference ΔF between the two opposite spin electron oscillations depends on the exchange splitting energy E_{ex}, which is generally proportional to the magnetization M in magnetic metals [27,28], we obtain

$$\begin{aligned}\Delta\rho =& 2A(B,T)\cos\left[2\pi\left(\frac{F}{B}+\phi'\right)\right]\\ &\times\cos\left[\pi\left(\frac{\alpha M(B,T)+\Delta_0}{B}+\mathcal{G}\right)\right],\end{aligned} \tag{5}$$

in which α is the exchange interaction constant, Δ_0 is the exchange splitting at $T = 0$, and $M(B, T)$ is explicitly a function of both temperature and magnetic field. This approach gives the possibility of including the exchange interaction of electrons with magnetic ions into a simple band structure model. The last term, $\pi(\frac{\alpha M(B,T)+\Delta_0}{B}+\mathcal{G})$, can lead to the beating patterns in oscillations at half-integer values, which is consistent with the observation that the nodal positions shift with temperature in NdAlSi.

With the above model, we can use the magnetization data $M(T)$, which traces the spin polarization of f electrons under the influence of the c-f exchange interactions, to reproduce the temperature dependent resistivity at various magnetic fields with the resulting expression (5). Due to the constant value of B, expression (5) could be simplified as $\Delta\rho = \cos(\frac{\alpha' M}{B}+\frac{\Delta_0'}{B}+\delta)(-AdM/dT)$, where A, α', Δ_0' and δ are constant parameters. The last term, $-AdM/dT$, is the correction to the amplitude, because the changes we observed in $A(B, T)$ are proportional to the changes in $-M(B, T)$. Furthermore, as shown in Fig. 1(b), the oscillatory resistivity data are well reproduced by the expression, which confirms that the observed oscillations arise from the dynamical coupling of the Weyl fermions and f electrons in NdAlSi. From the obtained α' (0.025 ± 0.001) (mol T emu^{-1}), Δ_0' (24 ± 2) (T), and the corresponding effective cyclotron mass m^* ($0.098m_0$, m_0 is the free-electron mass; see Fig. 9), the strength of the $4f$-Weyl fermion exchange interaction in NdAlSi is estimated to be 0.016 eV. It is higher than the experimental value in NdB_6 with a larger m^* [13]. Taking the aforementioned parameters, we have also simulated the oscillating $\Delta\rho$–B curve at 16 K using expression (5), and compared it with the experimental curve as shown in Fig. 2(d). Again, the good agreement between the theoretical and experimental curves proves that the origin of beating patterns of the SdH oscillations is rooted in the interplay of RD, Zeeman, and c-f exchange splitting.

Quantum oscillation were also observed in the magnetic field dependent specific heat of NdAlSi, as shown in Fig. 3(a). It is more directly connected to the modulation of the density of states (DOS) and being not directly related to electronic scattering. Here the most remarkable feature is that, unlike the SdH oscillations, the specific heat shows only a few oscillations in the intermediate field region before the system becomes fully polarized. After subtracting a smooth background, C_{osc} (B^{-1}) oscillating with a temperature independent frequency of 45 T is obtained; see Fig. 10(d) inset. Noticeably, the specific heat oscillation minima correlate with the maxima of SdH oscillations in MR [see Fig. 3(b) inset], due to the oscillatory behavior in specific heat characterized by the sine term [19].

We have also performed measurements of temperature dependent specific heat at various magnetic fields. The most intriguing feature obtained here is the saddlelike structure that evidences a superimposed oscillation due to the quantum oscillations of the DOS [Fig. 3(c)]. It should be pointed out that the oscillatory component of the total heat capacity is very small compared to the huge background arising from CEF splitting. To see the temperature variation of C_{osc} more clearly, we plot C_{osc} vs logarithmic temperature at selected magnetic fields in Fig. 3(d), after subtracting the contributions of the lattice and CEF. Here, an oscillatory character of the electronic specific heat with respect to magnetic field is clearly demonstrated.

Remarkably, the low temperature heat capacity data can be well fitted with an expression for activated behavior ($Ae^{-\Delta_\varepsilon/T}$) in the high field phase [see Fig. 4(a)], where the spins are entirely polarized by the external fields with ferromagneticlike correlations. This kind of activated behavior indicates the opening of a magnetic excitation gap in the PPM phase; see Fig. 4(b) [29]. Likewise, the drastic decrease of the low-

temperature resistivity under high fields may have the same origin. We have estimated the excitation gap Δ_ε by $\rho = Ae^{-\Delta_\varepsilon/T} + \rho_0$ [30], and have plotted it versus the corresponding magnetic field B in Fig. 4(b), along with that deduced from the heat capacity measurements. Despite the apparent difference in gap values, both estimations tend to go to zero at finite magnetic field ($B_c^* \sim 3$ T) rather than at zero field, as would be excepted for a field-polarized paramagnetic ground state. It should also be remarked that the critical field B_c^* value is slightly different from the critical field $B_c \sim 5.2$ T, indicating that the polarization occurs before the suppression of antiferromagnetic order, which is consistent with the scenario that the polarization destroys the antiferromagnetism in NdAlSi [11].

An extended temperature-field phase diagram of NdAlSi for $B//c$ is then established in Fig. 4(c). It shows clearly that the paramagnetic phase becomes polarized with increasing field strength and decreasing temperature, therein a crossover from a paramagnetic to a ferromagneticlike polarized state emerges. The temperature dependent oscillations occur in the crossover regime, as discuss above. In particular, the maximum amplitude of the spindlelike oscillations appears near a critical temperature T^*, which is just located at the so-called "boundary" between the PM and the PPM states [Fig. 4(c) main panel and inset], where a remarkable spin-splitting of the Fermi surface has occurred. This demonstrates again that all the unconventional behaviors observed in NdAlSi are strictly linked to the existence of the $c-f$ exchange splitting. During the magnetic polarization process of the localized $4f$ electrons, the two opposite spin states are further mixed by RD interactions, Zeeman, and CEF effects at the Fermi levels.

III. CONCLUSION

In summary, we have observed a different presentation of quantum oscillations in the temperature dependent resistivity and specific heat at a constant magnetic field in magnetic Weyl semimetal NdAlSi. Such oscillations only appear at the narrow field-induced crossover region from PM to PPM. We have proposed a phenomenological model to address the unique quantum oscillations by considering the spin-split Fermi surfaces originating from the strong Weyl fermion–f electron exchange interaction, in addition to the Zeeman and RD spin splittings. Whether such phenomena could be explicitly observed in the same R-Al-B series with other rare-earth elements, despite the detailed differences in spin configuration, and whether the effects could be generally realized in systems where an internal field generated by local moments that strongly depending on temperature, require further investigation.

ACKNOWLEDGMENTS

This work was supported by the National Natural Science Foundation of China (Grants No. 11874417, No. U1504107, No. 12141002, No. 11974389, No. 52088101, and No. 12274117), the Strategic Priority Research Program (B) of Chinese Academy of Sciences (Grants No. XDB33020100 and No. XDB33000000), the National Key Program of China (Grants No. 2022YFA1402200 and No. 2021YFA0718700), and Henan Center for Outstanding Overseas Scientists (No. GZS2023007). We would like to thank L. Yu, W.-L. Zhu, Y.-Y. Wang, M. Lv, and Y.-D. Gu for helpful discussions.

J.-F.W. and Q.-X.D. contributed equally to this work.

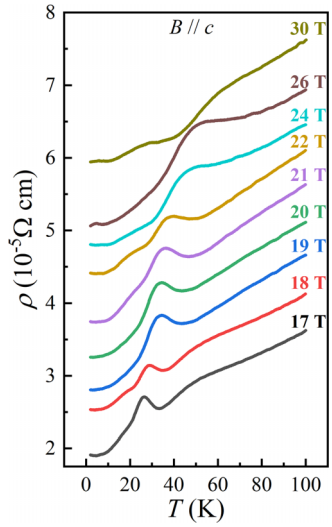

FIG. 5. Temperature dependent resistivity measured at higher magnetic fields (17–30 T) for $B//c$ axis. The oscillating character is not completely suppressed up to 30 T. The $\rho-T$ curves are vertically shifted by 0.45×10^{-5} Ω cm for clarity.

APPENDIX

Extended data and analysis are present in Figs. 5–14 and Table I.

Figure 10(a) displays $C(T)$ of NdAlSi obtained for 0–16 T. The specific heat is characterized by the large contribution of $4f$ electrons, C_{4f}. The increasing magnetic fields gradually suppressed the antiferromagnetic and ferrimagnetic transitions, however, the broad CEF Schottky peak moves to higher

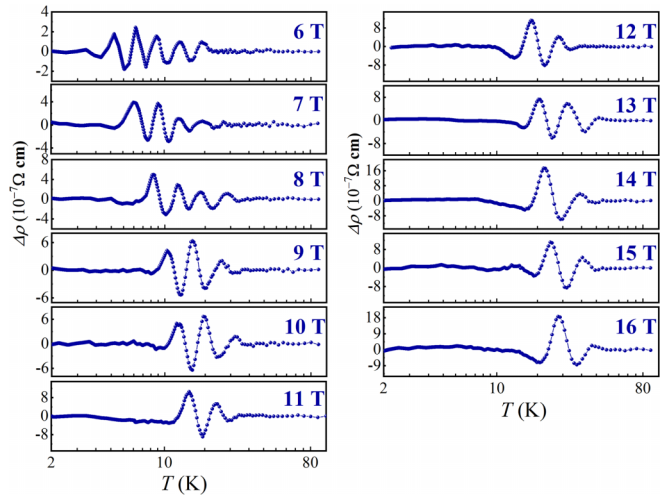

FIG. 6. Extracted $\Delta\rho-T$ oscillations under external magnetic fields (6–16 T). The spindlelike oscillation exhibits a log-periodic-like temperature dependence, shifts to a higher temperature, accompanying a slight enhancement of amplitude, but the number of oscillations decreases dramatically upon increasing magnetic field.

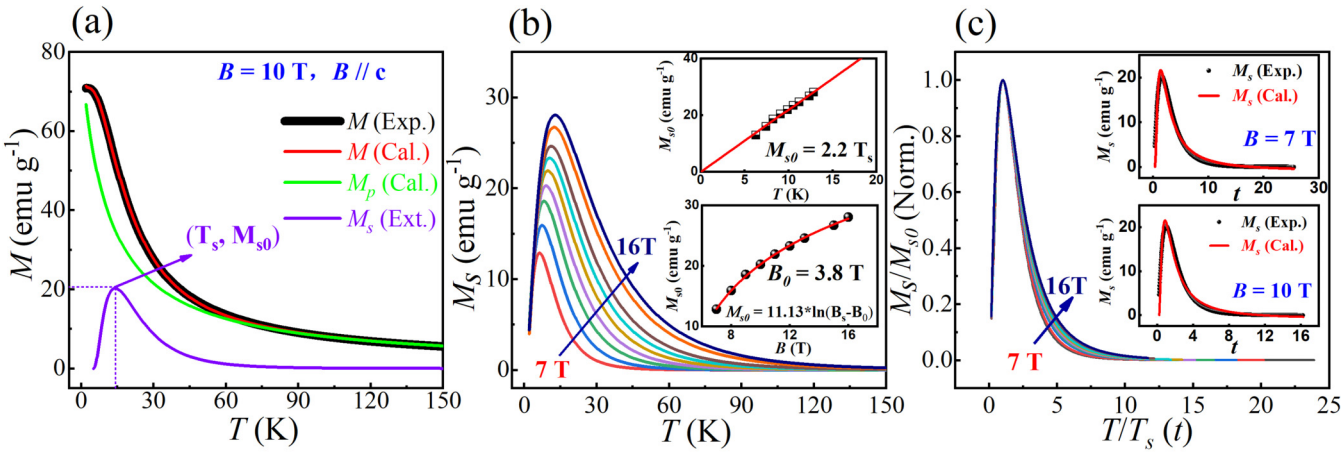

FIG. 7. Reproduction of the $\Delta\rho-T$ oscillations based on magnetization data. (a) Temperature dependent magnetization M [zero-field-cooled (ZFC)] for $B = 10$ T. By subtracting the Curie-Weiss term $M_p(T)$ (green line), the component of the spin polarization M_s (purple line) can be obtained. Two characteristic parameters, T_s and M_{s0}, were defined at the inflection point, as shown in the figure. (b) Extracted M_s-T curves for various magnetic fields (7–16 T). From the plot of M_{s0} against T_s (the upper inset), we then obtained the relation $M_{s0} = 2.2T_s$. It seems that there is an intrinsic relationship among the curves, so we try to plot M_s/M_{s0} vs T/T_s(t), as shown in (c), and find that all the curves overlap with each other for low temperature region. Slight deviations at elevated temperatures might be due to the appearance of the large CEF effect. This result means that all the M_s curves can be normalized by a formula $M_s/M_{s0} = a^*t^{-1.5*}\exp(-b/t) + c^*t^{0.5} + d$, where, the fitted four constant parameters of a, b, c, and d are 4.406 45, 1.237 06, 0.0615, and −0.315 17 respectively, $t = T/T_s = 2.2^*[11.13^*\ln(B - B_0)]^{-1*}T$, and $M_{s0} = 11.13^*\ln(B_s - B_0)$, obtained from the plots of M_{s0} vs T and M_{s0} vs B as in the insets of (b). Finally, we can obtain a $M(T)$ curve for any magnetic field only plus the Curie-Weiss term $C/(T+\Theta)$, as shown in (a) (red line). To check the accuracy of the simulation, we plotted both the calculated and measured results for comparison, as shown in the insets. Reproduction of the $\Delta\rho-T$ oscillations based on magnetization data for $B = 6$, 7, 8, 9, 10, and 13 T are shown in Fig. 1(b), which agree well with each other. The details are presented in the main text.

temperature, where very weak oscillations are superimposed. We estimate the C_{4f} by subtracting the phonon component $C_{\rm ph}$ from $C(T)$, assuming that the $C_{\rm ph}$ is equal to the specific heat of the nonmagnetic reference compound LaAlSi, as shown in the inset of Fig. 10(a). We find that, at zero field and high temperatures, the C_{4f} curve can be reproduced by considering that the tenfold degenerate $|J = 9/2\rangle$ level splits into a ground state doublet and four excited doublets with $\Delta = 4.1$ meV using the generic formula for a multilevel CEF scheme:

$$C_{\rm CEF}(T) = \frac{\left(\frac{R}{T^2}\right)\left[\sum_i g_i e^{-\Delta_i/T}\sum_i g_i\Delta_i^2 e^{-\Delta_i/T} - \left(\sum_i g_i\Delta_i e^{-\Delta_i/T}\right)^2\right]}{\left(\sum_i g_i e^{-\Delta_i/T}\right)^2},$$

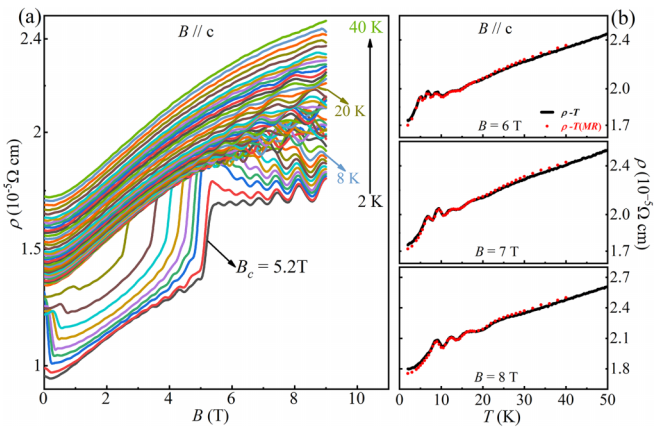

FIG. 8. Comparisons made between the extracted data (red dotted line) from (a) isothermal magnetoresistivity measurements (2–40 K) and (b) the directly measured $\rho(T)$ curves (back solid line).

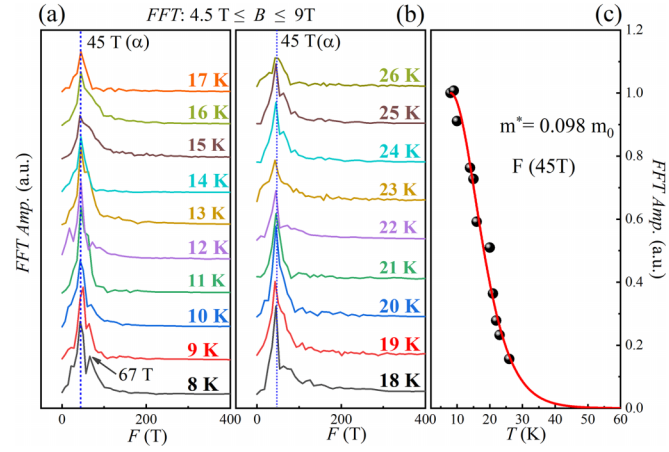

FIG. 9. Fast Fourier transform (FFT) spectra based on the SdH oscillations and the corresponding effective mass. (a), (b) The main spectral weight sitting at 45 T, showing no obvious temperature dependence; a weak peak located at about 67 T also can be identified. (c) FFT amplitude vs temperature, fitted with the thermal damping factor in Lifshitz-Kosevich (LK) formula.

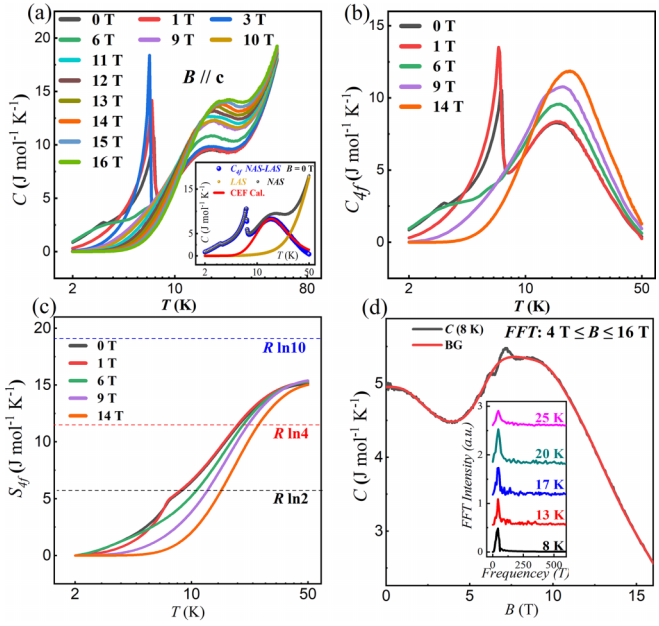

FIG. 10. Magnetic entropy and specific heat oscillations of NdAlSi. (a) The specific heat from 0 to 16 T. Inset: The $4f$ electrons contribution C_{4f} (blue) to the specific heat, obtained by subtracting the specific heat of LaAlSi (yellow) from that of $C(T)$ (gray). The red line is the calculation for $B = 0$ T using the CEF model with $\Delta = 4.1$ meV. (b) C_{4f} vs temperature for selected magnetic fields. (c) The magnetic entropy S_{4f}, by integrating C_{4f}/T with respect to T. (d) Magnetic field dependent $C(B)$ measured at $T = 8$ K. Inset: FFT spectra of the specific heat oscillation at selected temperature.

TABLE I. The fitted energy eigenvalue of Nd_{4f} at various fields based on CEF model with a ground state doublet and eight excited states.

Magnetic field (T)	0	9	10	11	12	13	14	15	16
Eigenvalue (meV)									
Δ_1	0	0	0	0	0	0	0	0	0
Δ_2	0	0	0	0	0	0	0	0	0
Δ_3	4.1	1.6	1.8	2.0	2.1	2.4	2.6	2.7	2.9
Δ_4	4.1	4.2	4.4	4.5	4.6	4.4	4.6	4.7	4.8
Δ_5	4.1	4.2	4.4	4.5	4.6	4.4	4.6	4.7	4.8
Δ_6	4.1	4.2	4.4	4.5	4.6	4.4	4.6	4.7	4.8
Δ_7	4.1	4.2	4.4	4.5	4.6	5.8	6.3	6.6	6.0
Δ_8	4.1	6.1	4.4	12.9	13.2	13.8	14.1	14.3	13.0
Δ_9	4.1	12.5	12.8	12.9	13.2	13.8	14.1	14.3	13.8
Δ_{10}	4.1	12.5	12.8	12.9	13.2	13.8	14.1	14.3	13.8

where g_i is the degeneracy of the ith excited level at energy Δ_i.

Figure 10(b) shows the $C_{4f}(T)$ for several magnetic fields. With increasing magnetic field, the λ-type peak is gradually suppressed, and the improved Schottky maximum shifts to a higher temperature. The CEF calculations presented by dotted curves and the energy eigenvalue for different magnetic fields, considering a ground state doublet and eight excited states, are summarized in Fig. 10 and Table I, respectively. Figure 10(c) shows the $4f$ electrons derived magnetic entropy S_{4f} by integrating C_{4f}/T with respect to T for various magnetic fields. At $B = 0$, S_{4f} reaches the value of 4.95 J mol^{-1} K^{-1} just above T_N (7.3 K), which approaches the $R \ln 2$ (5.76 J mol^{-1} K^{-1}), indicating that the two-phase transitions occur in a doublet ground state. Figure 10(d) shows

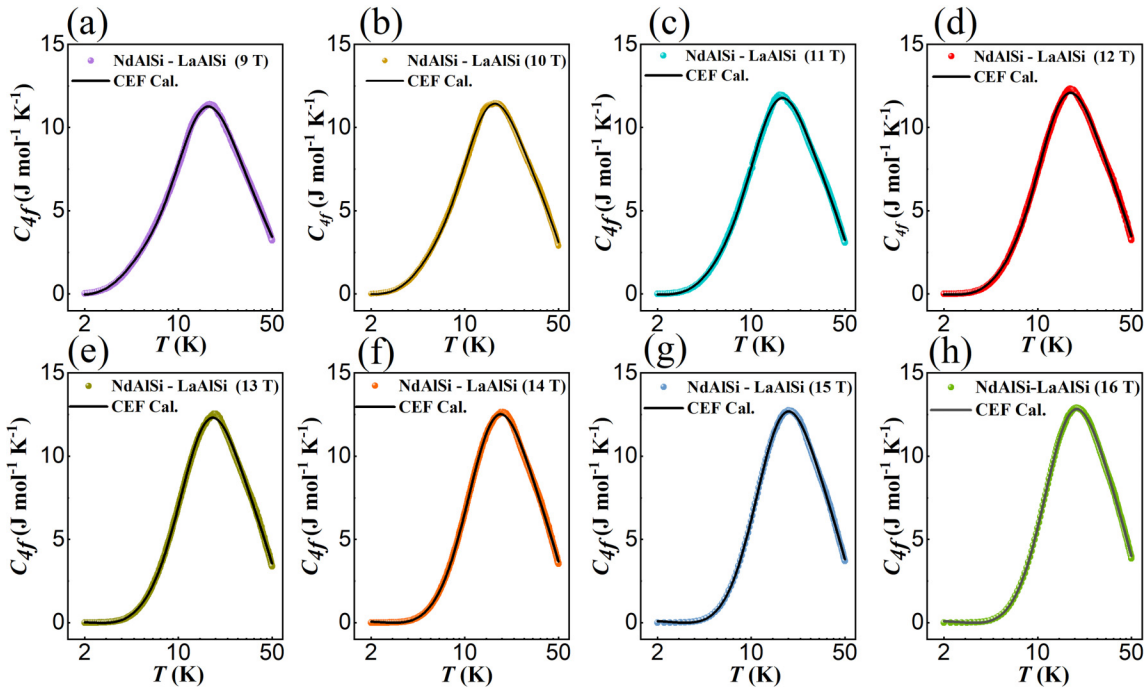

FIG. 11. Panels (a)–(h) are $4f$ electron contributions C_{4f} to the specific heat in NdAlSi and CEF fitting from 9 to 16 T, respectively.

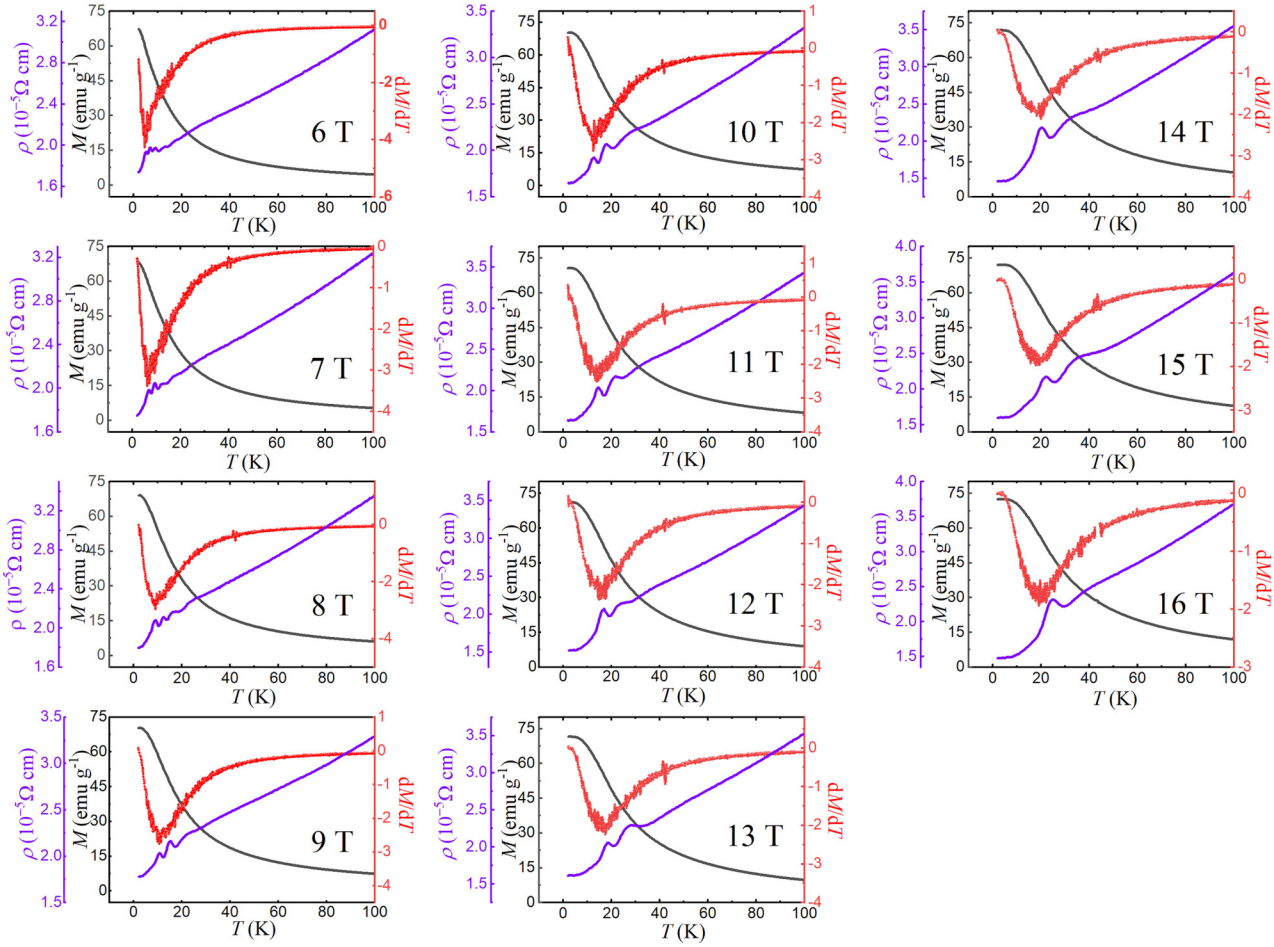

FIG. 12. Temperature dependent magnetization (M-T, black line), dM/dT (red line) and resistivity ($\rho-T$, purple) from 6 to 16 T. The $\rho-T$ oscillations are confined to the temperature range where the sample undergoes a change in the magnetization. Note here that neither in M-T data nor dM/dT could we identify any oscillation with temperature, possibly due to the huge magnetization background by Nd moments and the limited resolution of the high field viberating sample magnetometer.

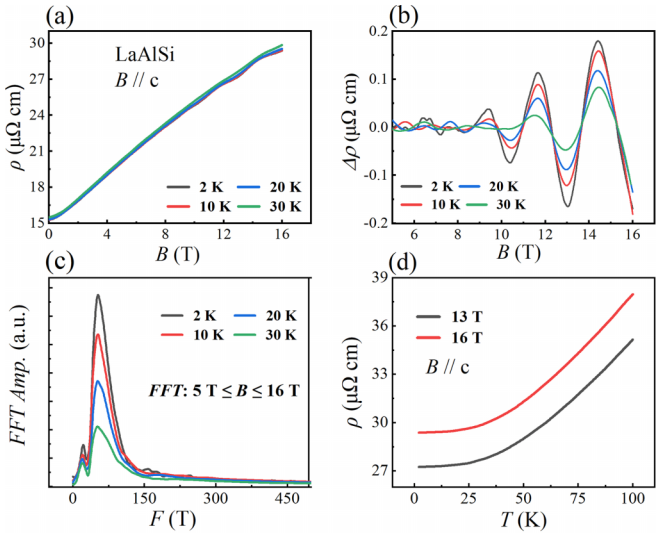

FIG. 13. Magnetoresistivity and SdH of isostructural nonmagnetic LaAlSi. (a) Isothermal magnetoresistance. (b) Extracted SdH oscillations. (c) FFT spectra of oscillatory $\Delta\rho$ at various temperatures. (d) Temperature dependent resistivity at 13 and 16 T, respectively.

the $C(B)$ at $T = 8$ K. An oscillation feature appears at about 4 T and disappears after the system is in the fully PPM state. More exactly, there are five contributions, i.e., the electronic C_e, phonon $C_{\rm ph}$, magnetic C_{4f}, Shottky-like $C_{\rm CEF}$, and

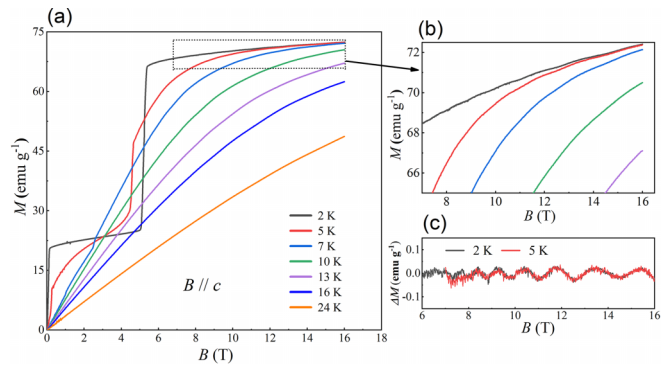

FIG. 14. (a) Isothermal M-H curves of NdAlSi up to 16 T for $B//c$. (b) The zoom-in part at low temperature and high field exhibit a tiny magnetization oscillation behavior. (c) The extracted de Haas-van Alphen at 2 and 5 K.

oscillatory component $C_{\rm osc}$, to the temperature and magnetic field dependencies of the specific heat in NdAlSi: $C(T,\ B) = C_e + C_{\rm ph} + C_m + C_{\rm CEF} + C_{\rm osc}$. By subtracting the other four contributions, we can obtain the specific heat oscillations $C_{\rm osc}$. For simplicity, the $C_{\rm osc}$ herein was obtained by subtracting a normalized smooth background. The typical $C_{\rm osc}$ oscillations and the corresponding FFT (fast Fourier transform) spectra are shown in Fig. 10(d) and its inset. Note that the obtained frequency of the specific heat oscillations is consistent with that of the SdH oscillations.

[1] G. Q. Chang, B. Singh, S.-Y. Xu, G. Bian, S.-M. Huang, C.-H. Hsu, I. Belopolski, N. Alidoust, D. S. Sanchez, H. Zheng, H. Lu, X. Zhang, Y. Bian, T.-R. Chang, H.-T. Jeng, A. Bansil, H. Hsu, S. Jia, T. Neupert, H. Lin, and M. Z. Hasan, Magnetic and noncentrosymmetric Weyl fermion semimetals in the *R*AlGe family of compounds (R = rare earth), Phys. Rev. B **97**, 041104(R) (2018).

[2] T. Suzuki, L. Savary, J. P. Liu, J. W. Lynn, L. Balents, and J. G. Checkelsky, Singular angular magnetoresistance in a magnetic nodal semimetal, Science **365**, 377 (2019).

[3] H.-Y. Yang, B. Singh, J. Gaudet, B. Lu, C.-Y. Huang, W.-C. Chiu, S.-M. Huang, B. Wang, F. Bahrami, B. Xu, J. Franklin, I. Sochnikov, D. E. Graf, G. Xu, Y. Zhao, C. M. Hoffman, H. Lin, D. H. Torchinsky, C. L. Broholm, A. Bansil, and F. Tafti, Noncollinear ferromagnetic Weyl semimetal with anisotropic anomalous Hall effect, Phys. Rev. B **103**, 115143 (2021).

[4] P. Puphal, V. Pomjakushin, N. Kanazawa, V. Ukleev, D. J. Gawryluk, J. Ma, M. Naamneh, N. C. Plumb, L. Keller, R. Cubitt, E. Pomjakushina, and J. S. White, Topological Magnetic Phase in the Candidate Weyl Semimetal CeAlGe, Phys. Rev. Lett. **124**, 017202 (2020).

[5] D. Destraz, L. Das, S. S. Tsirkin, Y. Xu, T. Neupert, J. Chang, A. Schilling, A. G. Grushin, J. Kohlbrecher, L. Keller, P. Puphal, E. Pomjakushina, and J. S. White, Magnetism and anomalous transport in the Weyl semimetal PrAlGe: Possible route to axial gauge fields, npj Quantum Mater. **5**, 5 (2020).

[6] M. Lyu, J. Xiang, Z. Mi, H. Zhao, Z. Wang, E. Liu, G. Chen, Z. Ren, G. Li, and P. Sun, Nonsaturating magnetoresistance, anomalous Hall effect, and magnetic quantum oscillations in the ferromagnetic semimetal PrAlSi, Phys. Rev. B **102**, 085143 (2020).

[7] Y. Sun, C. Lee, H.-Y. Yang, D. H. Torchinsky, F. Tafti, and J. Orenstein, Mapping domain-wall topology in the magnetic Weyl semimetal CeAlSi, Phys. Rev. B **104**, 235119 (2021).

[8] D. S. Sanchez, G. Chang, I. Belopolski, H. Lu, J.-X. Yin, N. Alidoust, X. Xu, T. A. Cochran, X. Zhang, Y. Bian, S. S. Zhang, Y.-Y. Liu, J. Ma, G. Bian, H. Lin, S.-Y. Xu, S. Jia, and M. Z. Hasan, Observation of Weyl fermions in a magnetic non-centrosymmetric crystal, Nat. Commun. **11**, 3356 (2020).

[9] P. Nikolic, Dynamics of local magnetic moments induced by itinerant Weyl electrons, Phys. Rev. B **103**, 155151 (2021).

[10] J. Gaudet, H.-Y. Yang, S. Baidya, B. Lu, G. Xu, Y. Zhao, J. A. Rodriguez-Rivera, C. M. Hoffmann, D. E. Graf, D. H. Torchinsky, P. Nikolic, D. Vanderbilt, F. Tafti, and C. L. Broholm, Weyl-mediated helical magnetism in NdAlSi, Nat. Mater. **20**, 1650 (2021).

[11] J. F. Wang, Q. X. Dong, Z. P. Guo, M. Lv, Y. F. Huang, J. S. Xiang, Z. A. Ren, Z. J. Wang, P. Sun, G. Li, and G. F. Chen, NdAlSi: A magnetic Weyl semimetal candidate with rich magnetic phases and atypical transport properties, Phys. Rev. B **105**, 144435 (2022).

[12] P. Fazekas, *Lecture Notes on Electron Correlation and Magnetism* (World Scientific, Singapore, 1999), Vol. 5.

[13] R. G. Goodrich, N. Harrison, and Z. Fisk, Fermi Surface Changes Across the Neel Phase Boundary of NdB_6, Phys. Rev. Lett. **97**, 146404 (2006).

[14] D. G. Seiler, W. M. Becker, and L. M. Roth, Inversion-asymmetry splitting of conduction band in Gasb from Shubnikov-De Haas measurements, Phys. Rev. B **1**, 764 (1970).

[15] D. G. Seiler, B. D. Bajaj, and A. E. Stephens, Inversion-asymmetry splitting of conduction-band in Insb, Phys. Rev. B **16**, 2822 (1977).

[16] S. I. Epstein, R. J. Higgins, D. H. Lowndes, F. Steglich, and J. F. Smith, Dehaas-Vanalphen scattering measurements on the reentrant superconductor $La_{1-X}Ce_XAl_2$, Phys. Rev. B **32**, 5683 (1985).

[17] Y. Nakanishi, T. Sakon, M. Motokawa, M. Ozawa, and T. Suzuki, De Haas-van Alphen study of the spin splitting of the Fermi surface in TbSb, Phys. Rev. B **69**, 024412 (2004).

[18] H. Su, X. Shi, J. Yuan, Y. Wan, E. Cheng, C. Xi, L. Pi, X. Wang, Z. Zou, N. Yu, W. Zhao, S. Li, and Y. Guo, Multiple Weyl fermions in the noncentrosymmetric semimetal LaAlSi, Phys. Rev. B **103**, 165128 (2021).

[19] D. Schoenberg, *Magnetic Oscillations in Metals* (Cambridge University Press, England, 2009).

[20] H. Murakawa, M. S. Bahramy, M. Tokunaga, Y. Kohama, C. Bell, Y. Kaneko, N. Nagaosa, H. Y. Hwang, and Y. Tokura, Detection of Berry's phase in a bulk Rashba semiconductor, Science **342**, 1490 (2013).

[21] J. Kunc, B. A. Piot, D. K. Maude, M. Potemski, R. Grill, C. Betthausen, D. Weiss, V. Kolkovsky, G. Karczewski, and T. Wojtowicz, Magnetoresistance quantum oscillations in a magnetic two-dimensional electron gas, Phys. Rev. B **92**, 085304 (2015).

[22] K. S. Novoselov, A. K. Geim, S. V. Morozov, D. Jiang, M. I. Katsnelson, I. V. Grigorieva, S. V. Dubonos, and A. A. Firsov, Two-dimensional gas of massless Dirac fermions in graphene, Nature (London) **438**, 197 (2005).

[23] W. Z. Zhou, T. Lin, L. Y. Shang, G. Yu, K. H. Gao, Y. M. Zhou, L. M. Wei, L. J. Cui, Y. P. Zeng, and S. L. Guo, Anomalous shift of the beating nodes in illumination-controlled $In_{1-x}Ga_xAs/In_{1-y}Al_yAs$ two-dimensional electron gases with strong spin-orbit interaction, Phys. Rev. B **81**, 195312 (2010).

[24] G. Grabecki, T. Dietl, J. Kossut, and W. Zawadzki, Quantum transport in semimagnetic HgMnTe inversion layers — Experiment and theory, Surf. Sci. **142**, 588 (1984).

[25] N. B. Brandt and V. V. Moshchalkov, Semimagnetic semiconductors, Adv. Phys. **33**, 193 (1984).

[26] J. Kossut, Chapter 5 band structure and quantum transport phenomena in narrow-gap diluted magnetic semiconductors, Semiconduct. Semimet. **25**, 183 (1988).

[27] G. Lonzarich and A. V. Gold, Temperature-dependence of exchange splitting in ferromagnetic metals. 1. Information from Dehaas-Vanalphen effect in iron, Can. J. Phys. **52**, 694 (1974).

[28] M. Springfold, *Electrons at the Fermi Surface*, edited by M. Springford (Cambridge University Press, Cambridge, UK, 1980).

[29] J. A. Sears, Y. Zhao, Z. Xu, J. W. Lynn, and Y.-J. Kim, Phase diagram of α-$RuCl_3$ in an in-plane magnetic field, Phys. Rev. B **95**, 180411(R) (2017).

[30] N. H. Andersen and H. Smith, Electron-magnon interaction and the electrical resistivity of Tb, Phys. Rev. B **19**, 384 (1979).